


# Cavitation Bubbles Generated by Vibrating Quartz Tuning Fork in Liquid $^4\text{He}$ Close to the $\lambda$ -Transition

Daniel Duda<sup>1</sup>  · Patrik Švančara<sup>1</sup> · Marco La Mantia<sup>1</sup> · Miloš Rotter<sup>1</sup> · David Schmoranzer<sup>1</sup> · Oleg Kolosov<sup>2</sup> · Ladislav Skrbek<sup>1</sup>

Received: 28 July 2016 / Accepted: 20 October 2016 / Published online: 28 October 2016  
© Springer Science+Business Media New York 2016

**Abstract** We report direct optical observation of cavitation bubbles in liquid helium, both in classical viscous He I and in superfluid He II, close to the  $\lambda$ -transition. Heterogenous cavitation due to the fast-flowing liquid over the rough surface of prongs of a quartz tuning fork oscillating at its fundamental resonant frequency of 4 kHz occurs in the form of a cluster of small bubbles rapidly changing its size and position. In accord with previous investigators, we find the cavitation threshold lower in He I than in He II. In He I, the detached bubbles last longer than one camera frame (10 ms), while in He II the cavitation bubbles do not tear off from the surface of the fork up to the highest attainable drive.

**Keywords** Liquid helium · Cavitation · Bubble dynamics · Tuning fork

## 1 Introduction

The understanding of cavitation in both classical and quantum liquids, or more generally—detailed microscopic mechanism of bubble nucleation in them, remains largely an open problem [1], although its phenomenological description in classical viscous liquids [2] is valued for practical engineering purposes. The difficulty of the detailed description of the nucleation mechanism lies in the area between the validity of the continuum hypothesis and the individual particle approach; hence, quantum mechanics has to play an important role not only in quantum fluids but even in the

---

✉ Daniel Duda  
prog.dan@seznam.cz

<sup>1</sup> Faculty of Mathematics and Physics, Charles University in Prague, Ke Karlovu 3, 121 16 Prague, Czech Republic

<sup>2</sup> Physics Department, Lancaster University, Lancaster LA1 4YB, UK

case of classical liquids [3]. To this end, liquid helium offers a unique opportunity to study this problem both in He I, which is a classical low-density liquid possessing very low kinematic viscosity [4], and in He II, which is a quantum liquid exhibiting the two-fluid behavior. One can hope to discern which aspects of cavitation are common and different in classical and quantum liquids, and subsequently, such studies ought to help in developing the detailed microscopic description of the nucleation problem [3].

This work extends our previous investigations of cavitation in liquid helium due to an oscillating quartz fork. In Ref. [5], we have shown that cavitation can easily be detected by monitoring the frequency sweeps across the resonant frequency of the fork, as the electrical response collapses when cavitation occurs. In Ref. [6], the analysis of our results based on the Bernoulli equation in He II suggested pure cavitation, albeit heterogeneous in nature. Moreover, based on the measured temperature dependence of the critical cavitation velocity that steeply increased (from about 0.6 m/s to about 2.1 m/s for a particular fork) on decreasing temperature within about 20 mK below the superfluid transition in the bulk, we concluded that in He I the vicinity of the fork is locally overheated and cavitation occurs here at a higher temperature than that at which the surrounding helium bath is kept. We speculated that the steep increase in the cavitation threshold just below the superfluid transition can be understood as a consequence of the high convective heat transfer efficiency in superfluid He II compared to He I. This explains why, in accord with the previous observations [1, 5–7], it is more difficult to reach the cavitation in He II than in He I.

Motivated by recent work by Qu et al. [8] reporting differences in the lifetime of bubbles in He I and in He II, in this work we focus on the size and shape of the cavitation bubbles produced heterogeneously by the flow enhancement by excrescences on the surface of the oscillating quartz fork in He I as well as in He II.

## 2 Experimental Setup

We use our cryogenic optical system for visualizing liquid helium flows by the particle tracking velocimetry [9]. The apparatus consists of a low-loss cryostat with the experimental volume situated at its bottom in a tailpiece of square cross section, with windows for optical access. A pair of pumps can cool the bath along the saturated vapor pressure curve down to  $\sim 1.3$  K. The illumination is realized by a pulsed laser beam defocused by a cylindrical lens into a plane normally illuminating small tracer particles, which are not used in this study. A camera with telemetric lens and  $2\times$  extender has frequency 100 Hz and exposure time 9.998 ms (followed by  $2\ \mu\text{s}$  delay needed for readout and preparing the electronics), and it is positioned perpendicular to the plane illuminated by the laser.

The used quartz tuning fork has the resonance frequency  $f_0 = 4186$  Hz at 2 K, and the prongs have length  $L = 19.7$  mm, width  $W = 2.2$  mm and thickness  $T = 0.8$  mm, which are much larger than the viscous penetration depth  $\delta = \sqrt{2\nu/\omega} \approx 1\ \mu\text{m}$ . The fork constant,  $a$ , which characterizes its geometry and piezoelectric behavior, is measured to be  $a = 3.43 \cdot 10^{-5}$  C/m (the meaning of  $a$  and its determina-

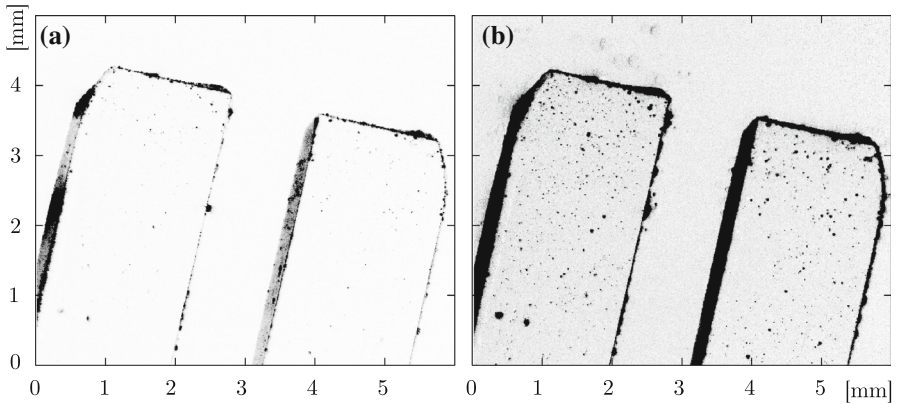


**Fig. 1** An example of acquired images of the fork with no drive: **a** in He II—note small particles of dirt used to measure the velocity; **b** in He I—the image has been darkened in order to highlight the bubbles appearing due to boiling near the fork surface overheated by the laser, confirming the presence of He I

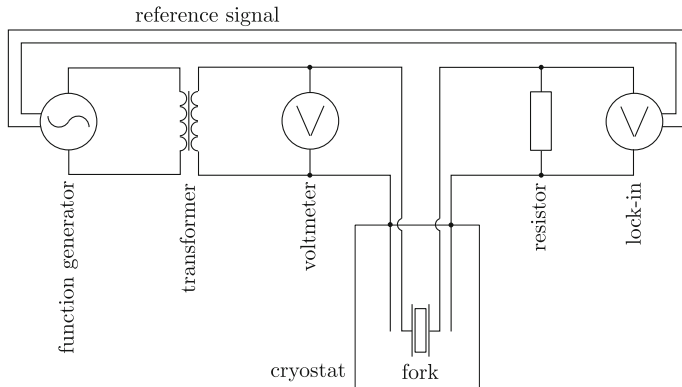


**Fig. 2** Scheme of fork electrical connection. The AC signal up to  $7.07 \text{ V}_{\text{rms}}$  is provided by a function generator, transformed up to a maximum  $U = 129.4 \text{ V}_{\text{rms}}$  and checked by a voltmeter. The current through the fork is measured by a lock-in amplifier as a voltage drop on a  $984 \Omega$  resistor

tion can be found in [10]). The fork is situated parallel to the laser plane, with its prongs aiming up with a small deviation of about  $13^\circ$  from vertical direction, see Fig. 1. Note in passing that all presented images are negatives of the captured ones.

The fork is driven by a function generator, and its response is measured by a lock-in amplifier; see Fig. 2. The maximum force we can achieve is  $F = aU \approx 4.4 \text{ mN}_{\text{rms}}$ . The velocity of the fork can be determined by two ways: (i) The velocity  $v$  is proportional to measured current  $I$ ;  $v = I/a$ , and this method is commonly used; and (ii) we use elongated or “motion-blurred” images of small particles of dust at the surface of the moving fork, which are clearly visible thanks to the side illumination, see Fig. 1. The duration of the laser pulse,  $\sim 0.4 \text{ ms}$ , exceeds one entire fork cycle period,  $0.24 \text{ ms}$ . The velocity found this way is slightly (up to about 20%) higher. The discrepancy

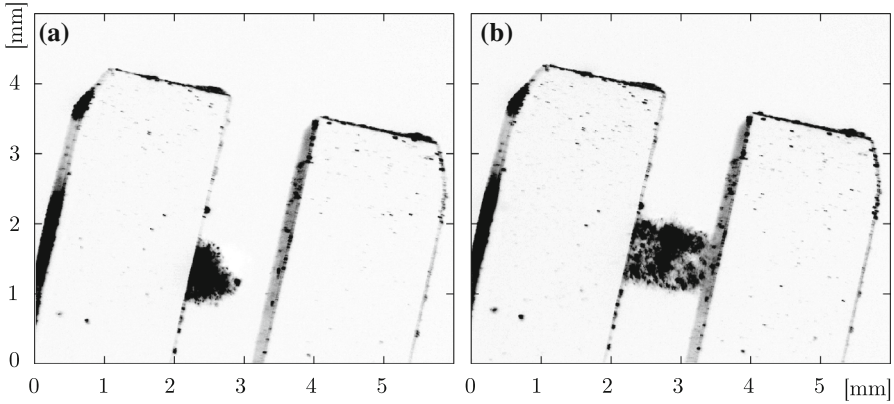


**Fig. 3** Fork under the same drive  $129 V_{\text{rms}}$  in **a** He II, rms velocity of the fork tips  $576 \text{ mm/s}$ , and **b** in He I, rms velocity  $528 \text{ mm/s}$

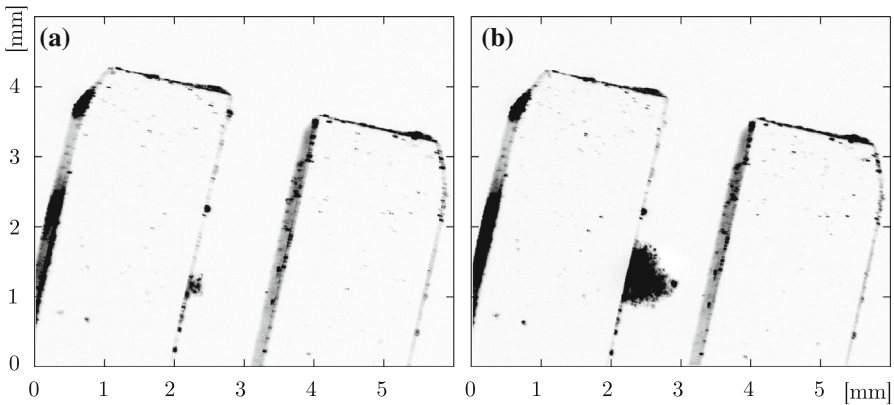


**Fig. 4** Fork at the same bulk temperature  $2.17 \text{ K}$ , i.e., in He II, but under different drives: **a**  $36.9 V_{\text{rms}}$ , rms fork tip velocity  $309 \text{ mm/s}$ ; **b**  $129 V_{\text{rms}}$ ,  $576 \text{ mm/s}$

is, however, not essential here; its most likely reason is either the finite value of the resistor (see Fig. 2) or the specific patterning of the electrodes deposited on the tuning fork.

### 3 Observations and Discussion

The surprising observation is that there is a cluster of small bubbles instead of one large nearly hemispherical bubble as minimization of the sum of the energy of surface tension and volume Gibbs energy would suggest, see Figs. 3 and 4. Note that although the camera exposure time,  $9.998 \text{ ms}$ , is much longer than the fork cycle period,  $0.24 \text{ ms}$ , the scene is illuminated only during the laser pulse, i.e., for  $\sim 0.4 \text{ ms}$ , corresponding to about 1.7 fork periods. This ensures capturing of the entire fork period, and on the other hand, the captured image is not a superposition of many peri-

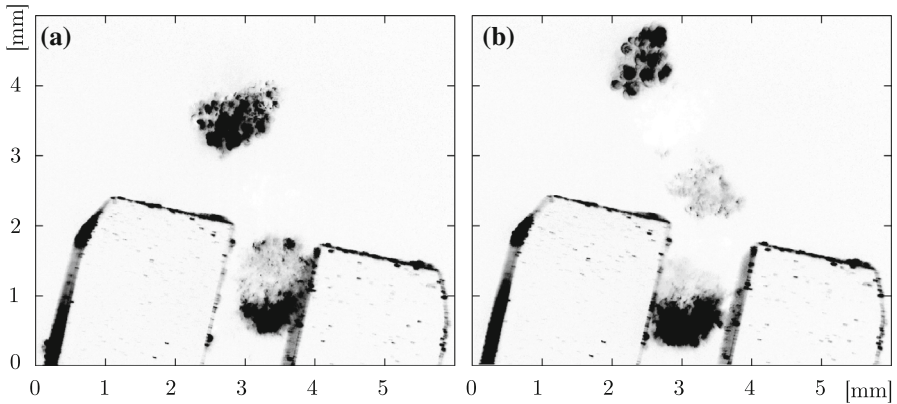


**Fig. 5** In He I at highest drives, the bubbles live longer than one fork cycle, and these bubbles then rise up. The **b** frame follows 10 ms after the **a** frame

ods. In He I, we sometimes observe that the bubbles live longer than one cycle; these bubbles then rise up as can be seen in Fig. 5. Such images strongly suggest that the observed bubbles form a real cluster and we do not observe a superposition of different bubbles produced during different fork cycles. In He II, the situation is different in that the bubbles do not tear off from the fork surface up to the highest attainable drive (Fig. 6).

The velocity of the fork versus the driving force is plotted in Fig. 7a. The fork moves fast enough to create the turbulent regime of flow past it, where the drag force  $F_D$  depends more or less quadratically on the velocity,  $F = F_D \propto v^2$ ; see the cases without cavitation in Fig. 7a. When cavitation occurs, the data points lie below this dependence because creation of bubbles consumes energy—this can be qualitatively interpreted as an additional braking force  $F_b$ —the difference between the applied drive force and the force, which would be needed to obtain the same velocity under the action of hydrodynamic drag force only, i.e.,  $F_b = F - Cv^2$ , where the prefactor  $C \approx 5.8 \cdot 10^{-3} \text{Ns}^2\text{m}^{-2}$  is the fitting parameter using the data of Fig. 7a. Note in passing that in He II the maximum energy losses can be carried away to the bulk by thermal counterflow of typical counterflow velocity up to a fraction of mm/s, i.e., much lower than the velocity of moving prongs.

We attempt to quantify the observed bubbles or clusters of bubbles by measuring their area  $A$  on each frame (by counting the pixels brighter than a chosen threshold). This leads to an effective radius  $r_{\text{eff}}$ , which the bubble would have, assuming its semispherical shape:  $r_{\text{eff}} = \sqrt{2A/\pi}$ . The effective radius of the bubble (or cluster of bubbles) is plotted versus the additional braking force in Fig. 7b. Although there is a visible correlation, the points are too scattered to discern any functional dependence. On the other hand, the reported difference in cavitation properties in He I and in He II is clearly visible: A fixed size bubble produces higher braking force in He II than in He I. The reason of this difference is unclear but might be connected either with the slightly larger surface tension of He II [4] or with quantized vorticity attached to cavitation bubbles.

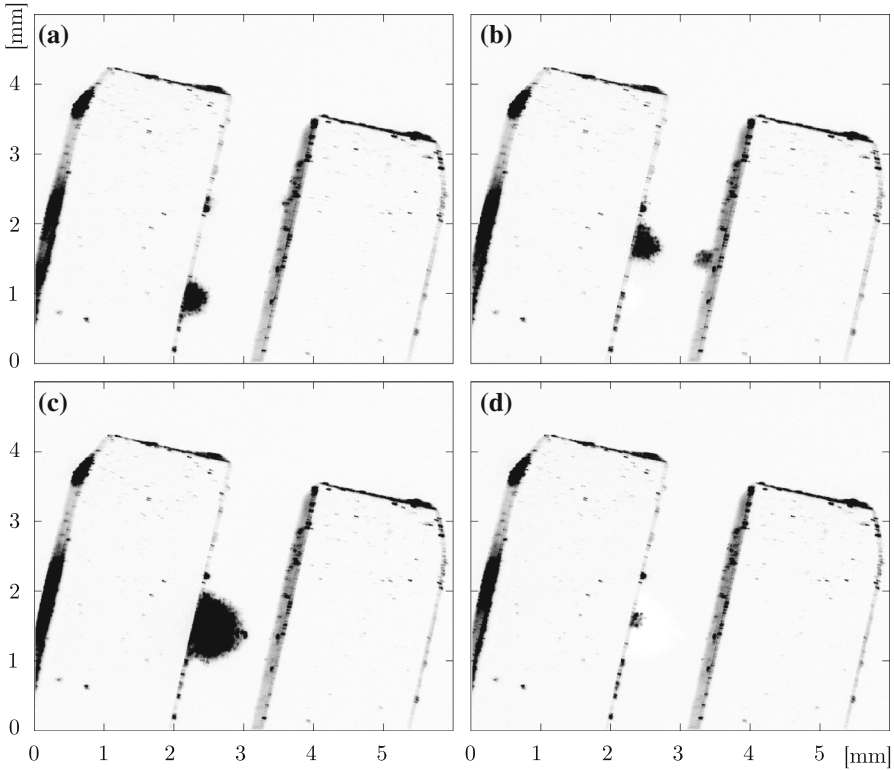


**Fig. 6** Four consecutive images (taken at intervals of 10 ms) of the cavitation bubbles in He II, fork drive  $129 V_{rms}$ , rms fork tip velocity 573 mm/s

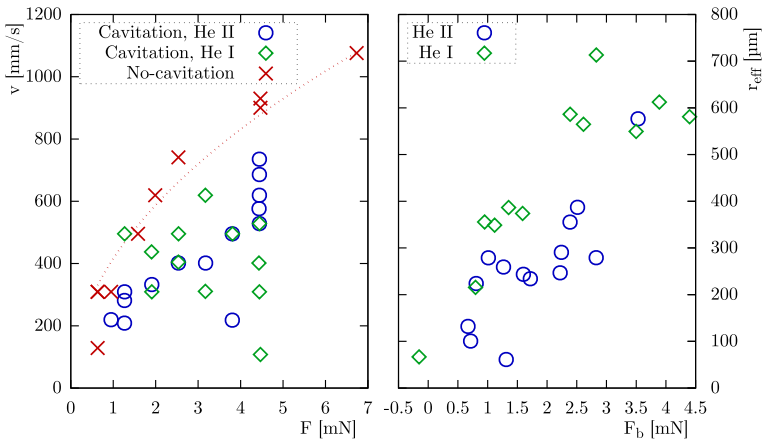


**Fig. 7** *Left* Measured velocity of prongs plotted versus applied force. The cases when the cavitation did not occur (*red crosses*) approximately follow the expected dependence  $F_D \propto v^2$  (*dotted line*) for the turbulent regime. *Right* Effective radius  $r_{eff}$  of observed cavitation bubbles as a function of the added braking force  $F_b$ , evaluated as explained in the text (Color figure online)

## 4 Conclusions

By using the fast optical camera, we have directly observed heterogeneous cavitation in flow of He I and He II due to oscillating quartz fork, on both sides of the  $\lambda$ -transition. Typically, a cluster of small bubbles is produced rather than one bigger hemispherical bubble, and the position, size and shape of such a cluster changes from frame to frame. The produced bubbles are at first look similar in He I and in He II; however, cavitation threshold is lower in He I than in He II. Once nucleated, bubbles live longer in He I than in He II and can rise up in the bulk from the place of their nucleation. Additionally, under otherwise identical conditions the nucleated bubbles brake the motion of the fork's prongs more in He II than in He I.

**Acknowledgements** We thank Bohumil Vejr and Martin Jackson for valuable help. We acknowledge the support of the Czech Science Foundation—GAČR 16–00580S; D. D. also acknowledges the support of Charles University—GAUK 1968214 and D. S. also acknowledges institutional support under UNCE 2040.

## References

1. S. Balibar, J. Low Temp. Phys. **129**, 363 (2002)
2. D.W. Oxtoby, J. Phys. Condens. Matter **4**, 7627 (1992)
3. R.D. Finch, Phys. Fluids **12**, 1775 (1969)
4. R.J. Donnelly, C.F. Barenghi, J. Phys. Chem. Ref. Data **27**, 1217 (1998)
5. M. Blažková, T.V. Chagovets, M. Rotter, D. Schmoranzler, L. Skrbek, J. Low Temp. Phys. **150**, 194 (2008)
6. M. Blažková, D. Schmoranzler, L. Skrbek, Low Temp. Phys. **34**, 298 (2008)
7. H.J. Maris, S. Balibar, M.S. Pettersen, J. Low Temp. Phys. **93**, 1069 (1993)
8. A. Qu, A. Trimeche, P. Jacquier, J. Grucker, Phys. Rev. B **93**, 174521 (2016)
9. M. La Mantia, T.V. Chagovets, M. Rotter, L. Skrbek, Rev. Sci. Instrum. **83**, 055109 (2012)
10. R. Blaauwegeers, M. Blažková, M. Človečko, V.B. Eltsov, R. de Graaf, J. Hosio, M. Krusius, D. Schmoranzler, W. Schoepe, L. Skrbek, P. Skyba, R.E. Solntsev, D.E. Zmeev, J. Low Temp. Phys. **146**, 537 (2002)